Briefings in Bioinformatics, 2025, **26(6)**, bbaf636
https://doi.org/10.1093/bib/bbaf636
Problem Solving Protocol

Prompt-based multimodal representation learning for drug repurposing

Jinliang Liu[1,2], Kaicheng U[3], Dhruv Rana[4], Sophia Meixuan Zhang[5], Jiahui Yu[4], Sen Yang[6], Bo Jin[7], Xiyue Wang[8], Zongxin Yang[9,*], Hongping Tang[10,*], Junhan Zhao[9,12,*]

[1]School of Computer Science and Artificial Intelligence, Zhengzhou University, No. 100 Science Avenue, Zhengzhou, Henan 450001, China
[2]Centre for Artificial Intelligence, University of Technology Sydney, 15 Broadway, Ultimo, NSW 2007, Australia
[3]Tri-Institutional Computational Biology & Medicine, Weill Cornell Medicine, 445 East 69th Street, New York, NY 10021, United States
[4]NYU Department of Psychology, 6 Washington Pl, New York, NY 10003, United States
[5]Department of Pediatrics, Memorial Sloan Kettering Cancer Center, 1275 York Avenue, New York, NY 10065, United States
[6]Independent Researcher
[7]Xinda College of Economics and Humanities, Shanghai International Studies University, 999 Dongtan Avenue, Chongming District, Shanghai, China
[8]College of Biomedical Engineering, Sichuan University, No. 24 South Section 1, Yihuan Road, Chengdu, Sichuan 610065, China
[9]Department of Biomedical Informatics, Harvard Medical School, 10 Shattuck Street, Boston, MA 02115, United States
[10]Department of Pathology, Shenzhen Maternity and Child Healthcare Hospital, Women and Children's Medical Center, Southern Medical University, Shenzhen, Guangdong 518042, China
[11]Department of Biostatistics, Harvard T.H.Chan School of Public Health, 677 Huntington Ave, Boston, MA 02115, United States
[12]Present address: Department of Pediatrics, the University of Chicago, 5721 South Maryland Avenue Chicago, IL, 60637, United States

*Corresponding authors. Junhan Zhao, Department of Biomedical Informatics, Harvard Medical School; Present address, Department of Pediatrics, Section of Biomedical Informatics, the University of Chicago, 5721 South Maryland Avenue Chicago, IL, 60637, United States. E-mail: junhan_zhao@hms.harvard.edu, junhanzv@uchicago.edu; Hongping Tang, Department of Pathology, Shenzhen Maternity and Child Healthcare Hospital,Women and Children's Medical Center, Southern Medical University, Shenzhen, Guangdong, China. E-mail: tony1998@126.com; Zongxin Yang, Department of Biomedical Informatics, Harvard Medical School, 25 Shattuck Street, Boston, MA 02115, United States. E-mail: zongxin_yang@hms.harvard.edu

Abstract

Drug repurposing significantly reduces development costs and shortens research cycles, making it a critical strategy in drug discovery. An emerging class of drug repurposing approaches applies deep learning to structural data. However, these methods often depend on static representations of molecular and protein structures, which may not fully capture the dynamic character of compound–protein interactions. To address these challenges and enhance the accuracy of compound–protein interaction predictions, we introduce an innovative prompt-based multimodal representation learning framework that dynamically encodes task-specific contextual information for drug repurposing. Specifically, the framework includes a dynamic prompt generation module that adaptively creates receptor-specific prompts and a prompt calibration module for effective multimodal feature integration and optimization. When applied to identifying FDA-approved drug candidates targeting G-protein-coupled receptors, our method achieved a 7.4% improvement in mean absolute error compared with state-of-the-art methods, with up to a 25.1% improvement for specific target-of-interest. By demonstrating potential in repurposing non-opioid treatments without the risk of addiction for safe pain management, our method has the capacity to advance drug discovery and meet a wide range of therapeutic needs.

Keywords: prompt learning; multimodality; representation learning; drug repurposing

Introduction

Artificial intelligence (AI) has rapidly transformed drug discovery, particularly in drug repurposing, allowing a faster, more cost-effective and precise identification of therapeutic candidates [1–3]. Traditional drug development pipelines are characterized by high costs, lengthy timelines, and low success rates, highlighting the necessity of AI in addressing these challenges. Early work by Schneider and Schneider [4] introduced deep generative models for *de novo* molecular design, demonstrating AI's ability to efficiently explore extensive chemical spaces. Jin *et al.* [5] advanced this approach by developing a hierarchical graph-based deep generative model that incorporated structural motifs to generate chemically valid and diverse molecules. More recently, Brown *et al.* [6] and Raffel *et al.* [7] demonstrated the potential of large language models in natural language processing (NLP), highlighting their applicability for a range of tasks. Zhang *et al.* [8] applied prompt-based language models to synthetic lethality tasks in cancer drug discovery, highlighting the synergy between AI-driven molecular design and NLP techniques. In parallel, progress in AI-based protein structure prediction has significantly improved understanding of drug–target interactions. Jumper *et al.* [9] and Senior *et al.* [10] introduced AlphaFold2 (AF2), which delivers highly accurate 3D models of protein conformations. Baek

Received: June 5, 2025. **Revised:** September 18, 2025. **Accepted:** October 23, 2025
© The Author(s) 2025. Published by Oxford University Press.
This is an Open Access article distributed under the terms of the Creative Commons Attribution-NonCommercial License (https://creativecommons.org/licenses/by-nc/4.0/), which permits non-commercial re-use, distribution, and reproduction in any medium, provided the original work is properly cited. For commercial re-use, please contact reprints@oup.com for reprints and translation rights for reprints. All other permissions can be obtained through our RightsLink service via the Permissions link on the article page on our site—for further information please contact journals.permissions@oup.com.

et al. [11] further employed AF2 for modeling protein complexes for unveiling drug–target interaction mechanisms. This progress builds on foundational benchmarking studies by Kryshtafovych et al. [12], which assessed protein structure prediction methods for biomedical applications. Complementary work by Wang et al. [13] introduced AI-integrated docking pipelines, achieving improved accuracy in virtual screening processes. Additionally, the David Baker group [14] illustrated how AI-driven structural predictions advance the understanding of protein–protein interactions (PPIs) and compound–protein interactions (CPIs) for identifying novel targets and designing new treatments.

While previous drug repurposing efforts have explored a wide range of diseases, pain management remains a critical yet underexplored area of concern. This is largely due to the pervasive reliance on opioids, which, despite their efficacy, are associated with significant risks of addiction, tolerance, and severe side effects. These challenges underscore the urgent need for repurposing efforts to identify safer and more effective options for analgesia. Targeting G protein-coupled receptors (GPCRs), which play pivotal roles in numerous physiological processes and diseases, offers a promising avenue to address this pressing therapeutic challenge [15–18]. Approximately 34% of FDA-approved drugs target GPCRs [19], including well-characterized families such as opioid receptors (μ, δ, κ), cannabinoid receptors (CB_1, CB_2), and prostaglandin receptors, all key mediators in pain signal transduction [20–22]. Despite their therapeutic relevance, GPCRs-focused drug discovery remains protracted and expensive, often exceeding 10 years and 1 billion, with success rates below 10% [23, 24]. Foundational structural biology efforts clarified key GPCR activation mechanisms [16, 17], while Venkatakrishnan et al. [25] identified structural signatures that modulate GPCRs behavior. Recent work [18, 26] highlights the elusive nature of GPCRs conformational states and the need for AI approaches integrating dynamic structural data. Other efforts [27, 28] show how structure-based models can expedite GPCRs drug discovery.

Computational approaches for drug repurposing can be broadly categorized into four main methodological frameworks, each with distinct advantages and limitations. **Network-based methods** leverage biological networks such as PPI networks and drug–target networks to identify potential drug–disease connections through network proximity analysis [29]. While these approaches excel at capturing systemic biological relationships and can identify indirect drug effects, they often suffer from incomplete network data and may miss novel mechanisms not represented in existing networks. **Structure-based methods** utilize 3D molecular structures for virtual screening and molecular docking to predict drug–target interactions [30]. Although these methods provide mechanistic insights and can handle novel targets, they are computationally intensive and may be limited by protein flexibility and binding site dynamics. **Machine learning (ML)-based methods** have emerged as powerful tools, ranging from traditional algorithms to deep learning approaches that can automatically learn complex patterns from large-scale molecular and biological data [31]. These methods demonstrate superior performance in handling high-dimensional data and can discover nonlinear relationships, but they often suffer from limited interpretability and require extensive training data. **Fuzzy logic-based methods** employ fuzzy set theory to handle uncertainty and imprecision in biological data, enabling robust decision-making in drug discovery [32]. While these approaches are well-suited for dealing with noisy biological data and can incorporate expert knowledge, they may lack the sophistication needed for complex pattern recognition in high-dimensional molecular spaces. Recent breakthroughs further demonstrate the rapid evolution of computational drug repurposing. Le et al. [33] showcased ML's transformative impact on carcinogenicity prediction, integrating diverse AI approaches from compound screening to clinical optimization, addressing traditional assay limitations through innovative computational toxicology frameworks. Similarly, advanced graph neural networks like EmerGNN [34] employ flow-based architectures to predict drug–drug interactions in emerging drugs, effectively leveraging biomedical networks to capture complex relational patterns that traditional methods miss, particularly for compounds with limited experimental data. These advances underscore the field's progression toward more sophisticated, multifaceted computational approaches. Motivated by this critical challenge, a recently groundbreaking method [15] successfully demonstrated the promise of a deep learning framework that integrates molecular imaging and protein 3D structural representations to identify repurposable drugs for pain management.

Despite these advances, significant challenges remain. Many AI models still rely on analyzing representations extracted from single modality, such as molecular structures or protein sequences, failing to capture CPIs interactions [9, 35]. Zhang et al. [36] highlighted the limitations of such embeddings for molecular dynamics, underscoring the need for more innovative solutions. Prompt learning, a learning paradigm that guides model behavior through task-specific prompts or contextual cues, has revolutionized AI by effectively unlocking the potential of pretrained models through carefully designed prompts. Previous studies leveraged NLP and demonstrated its remarkable effectiveness in various downstream tasks [6, 7]. Language-based prompting mechanisms featured broader applicability for NLP architectures across biomedical tasks, such as pharmacological ontologies [37, 38]. Zhang et al. [8] further extended this paradigm by showing how prompt-driven architectures improve interpretability in molecular prediction tasks such as synthetic lethality detection. Following the established paradigm of prompt-based learning in NLP [39, 40], where prompts serve as contextual cues that shape model behavior, our approach employs dynamic prompts in the molecular domain. These learnable components adaptively highlight receptor-specific molecular patterns, paralleling how textual prompts guide language models toward specific tasks. Inspired by these successes, we propose to introduce prompt learning into drug repurposing to address the challenge of capturing dynamic characteristics of drug–protein interactions. Differentiating from conventional prompt tuning that relies on fixed textual prompts, our method introduces visual prompts [41] as dynamically generated receptor-specific features, allowing the framework to model the complex spatial and chemical properties of molecular interactions.

In response, we propose a novel Dynamic Prompt Guided Network (DPGNet) tailored for GPCRs, incorporating two key innovations. First, as shown in Fig. 1, a dynamic prompt block (DPB) enhances model adaptability by encoding domain-specific cues [6, 7, 37]. Specifically, our DPB consists of a prompt synthesis module (PSM) that adaptively generates receptor-specific prompts through learnable components, and a prompt calibration module (PCM) that effectively integrates these prompts with molecular features through a specialized transformer architecture. This dual-module design enables our model to capture the complex drug–GPCR interactions with high precision. Second, we employ multimodal feature fusion, integrating 2D molecular data, pretrained protein embeddings, and 3D structural insights to improve receptor–ligand predictions [35, 36]. This comprehensive

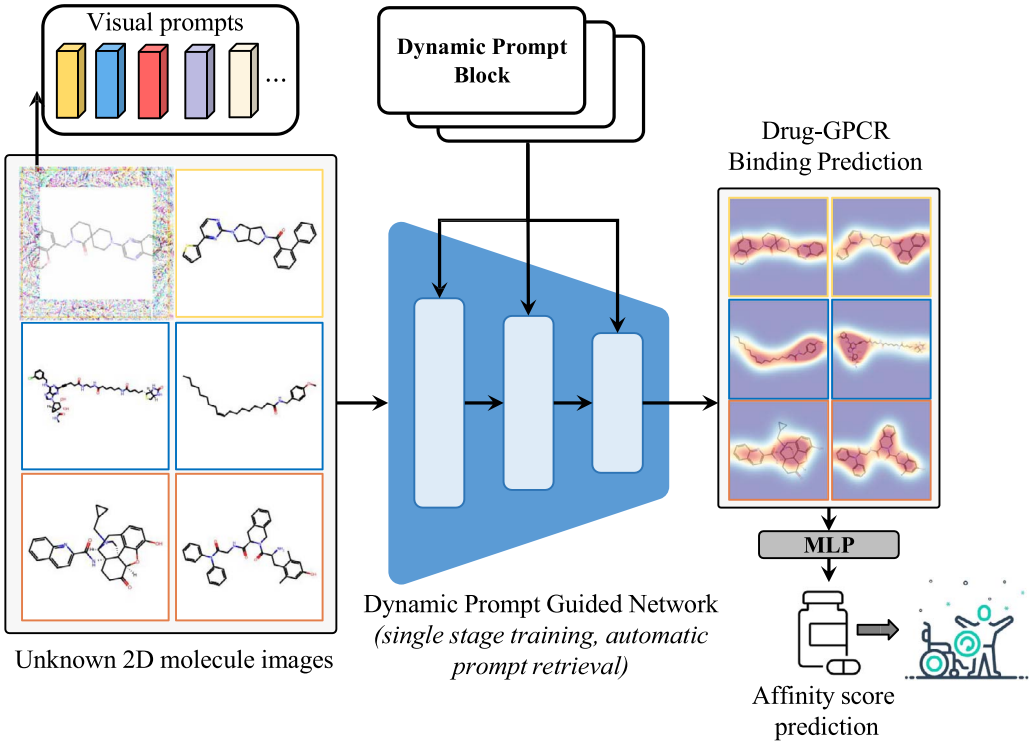

Figure 1. Dynamic prompt-based multi-modal framework for drug repurposing using adaptive dynamic prompt blocks to process 2D molecular images and predict drug-GPCR binding affinity.

framework is inspired by several pioneering works, including Li *et al.* [42], Wang *et al.* [43], and the groundbreaking AlphaFold2 (AF2) [9, 11].

Our preliminary results show significant improvements in mean absolute error (MAE) on GPCR datasets, achieving 0.189 MAE on the top-20 GPCR dataset and 0.179 MAE on the pain-related GPCR dataset, representing improvements of 35.9% over ChemBERT (0.295) and 25.1% over ImageMol (0.239). On challenging targets such as HRH3 (MAE: 0.148) in the top-20 GPCR dataset and 5HT1A (MAE: 0.145) in the pain-related GPCR dataset, our method achieves state-of-the-art performance, demonstrating superior predictive capability on therapeutically relevant receptors. These results highlight the practical potential of our framework in advancing GPCR-targeted drug discovery. Our findings align with Stein [20] and Willoughby *et al.* [44], who emphasize the urgent need for safer analgesics. The integration of prompt learning, multimodal data, and AI-based structural predictions reflects the shift toward context-aware, data-driven drug repurposing.

Datasets and methods

Datasets

To evaluate generalizability, we employed two comprehensive GPCR datasets, with summary characteristics shown in Table 1 and detailed statistics in Table 2.

Top-20 GPCR dataset: In this study, we used the Top-20 GPCR dataset proposed by Yang *et al.* [15]. This dataset contains 71 757 ligand–GPCR interaction pairs, meticulously curated from the ChEMBL and BindingDB databases, with a focus on interactions featuring reported Ki values. Rigorous preprocessing steps were applied to eliminate duplicates by matching InChIKey and UniProt ID entries. For interaction pairs with multiple reported activity values, the values were averaged. The processed dataset presents a concentrated distribution of activity values, with 76.6% of the compounds (55 001 in total) exhibiting activity values in the range of $[6, 9]$, and an overall mean activity value of 7.18.

Pain-related GPCR dataset: We also utilized the pain-related GPCR dataset proposed by Yang *et al.* [15], which comprises 33 212 ligand-GPCR interaction pairs, focusing on 13 GPCRs involved in pain modulation. The activity value distribution in this dataset follows a similar pattern, with 74.9% of compounds (25 826 in total) exhibiting activity values in the range of $[6, 9]$ and an overall mean activity value of 7.28. For the classification task, we employed a subset of 10 816 ligand–GPCR pairs specifically labeled as agonists or antagonists. Consistent with the original study, we excluded CCR2 from this analysis due to its exclusive antagonistic interactions, ensuring an unbiased evaluation of the model.

Metric: In this study, we followed the evaluation methods proposed by Yang *et al.* [15], using MAE and root mean square error (RMSE) as the primary metrics for model performance. MAE measures the average absolute deviation between predicted and actual values, while RMSE penalizes larger errors more heavily, providing a more stringent evaluation of the model. To ensure consistent scaling of these metrics, we applied Min-Max normalization to the input data, rescaling feature values to the range of $[-1, 1]$. This normalization reduced feature range discrepancies, enhanced model training stability, and improved numerical robustness. For data splitting, we allocated 70% of the samples from both the Pain-Related GPCR and Top-20 GPCR datasets to the training set, with the remaining 30% used for testing.

Methods

In this paper, we present DPGNet, a novel deep learning framework for CPI prediction, as illustrated in Fig. 2. We extract *multi-scale feature* representations at different spatial resolutions

Table 1. Dataset statistics for GPCR CPI prediction experiments. Alt text: A summary table of the two GPCR datasets used. The top-20 GPCR dataset has 71 757 pairs and a mean pKi of 7.18. The pain-related GPCR dataset has 33 212 pairs and a mean pKi of 7.28. Both datasets show over 74 percent of activity values in the 6–9 pKi range

Dataset	Total pairs	GPCR targets	Mean pKi	Activity range	Focus
Top-20 GPCR	71 757	20	7.18	6–9 (76.6%)	General GPCR discovery
Pain-related GPCR	33 212	13	7.28	6–9 (74.9%)	Pain management

Table 2. Statistical information of the top-20 GPCR dataset and Kinase dataset. Alt text: A breakdown of sample counts for the 20 GPCR targets (total 71 757) and the 10 Kinase targets (total 1046), including positive and negative kinase pair counts

GPCR dataset				Kinase dataset			
Target	**Samples**	**Target**	**Samples**	**Target**	**Samples**	**Positive**	**Negative**
5HT1A	4602	CNR2	3835	BTK	106	69	37
5HT2A	3874	DRD2	6897	CDK4	80	59	21
5HT2C	2470	DRD3	4880	EGFR	105	75	30
5HT6R	3635	DRD4	2554	FGFR1	108	76	32
5HT7R	2442	HRH3	3754	FGFR2	109	75	34
AA1R	4056	MC4R	1814	FGFR3	107	67	40
AA2AR	4572	OPRD	3617	FGFR4	107	59	48
AA2BR	1781	OPRK	3849	FLT3	110	79	31
AA3R	3970	OPRM	4471	KPCD3	109	68	41
CNR1	2923	OX2R	1761	MET	105	70	35
GPCR total: 71 757				**Total**	**1046**	**697**	**349**

($H/2^l \times W/2^l$ for level l), encoding molecular patterns from fine-grained atomic details to broader structural motifs. The motivation for this hierarchical approach is to capture molecular interactions across scales, ensuring that both local and global structural information is effectively represented. We employ a DPB to enhance the generalizability of DPGNet through adaptive prompt learning. Furthermore, we introduce a multidimensional enhancement strategy that integrates ImageMol and AlphaFold2. Through extensive experimentation, DPGNet demonstrates state-of-the-art performance in CPI prediction and outperforms existing models.

The overview of DPGNet framework

Our framework takes as input 2D molecular images ($I \in \mathbb{R}^{H\times W\times 3}$) representing drug compounds. A distinguishing component is the dynamic prompt generation mechanism, in which the PSM synthesizes receptor-specific visual prompts rather than relying on fixed textual inputs. These prompts, formulated as learnable feature components $\{P_i\}_{i=1}^N$, adapt to different GPCR subtypes and direct the model's attention toward relevant molecular patterns without the need for explicit receptor annotations. The network architecture of DPGNet follows a hierarchical feature extraction pipeline. Given an input molecular image $I \in \mathbb{R}^{H\times W\times 3}$, we first employ a 3×3 convolutional layer to extract low-level features $F_0 \in \mathbb{R}^{H\times W\times C}$. These features are then processed through a cascade of four Transformer blocks and three DPBs, where at each level l, the feature map dimensionality transforms as $F_l \in \mathbb{R}^{H/2^l\times W/2^l\times 2^l C}$. The final feature representations F_4 are aggregated via Global Average Pooling (GAP) to obtain a global descriptor $g \in \mathbb{R}^{8C}$, which is subsequently fed into a target classifier $\phi(\cdot)$ to predict the interaction score $s \in \mathbb{R}$.

Dynamic prompt block

The DPB is designed to adaptively generate receptor-specific feature representations. Our framework focuses on 13 pain-related GPCRs, with each receptor characterized by learnable dynamic prompt weights that are intrinsically activated based on molecular characteristics. This approach eliminates the need for explicit subtype annotations. The DPB consists of two core components: the PSM and the PCM, which will be described in detail in subsequent sections.

Prompt Synthesis Module: Accurate binding affinity prediction requires capturing receptor-specific structural features in protein–ligand interactions. To address this, we propose the PSM, which dynamically generates context-aware prompts using learnable components and attention-based weight allocation. Formally, given the lth block's input features $F_l \in \mathbb{R}^{H/2^l\times W/2^l\times 2^l C}$, PSM generates dynamic prompts through the following pipeline. First, to capture the global contextual information from the feature map, we utilize GAP to aggregate spatial features across all positions in F_l, which compresses the spatial dimensions into a channel-wise feature vector $v_g \in \mathbb{R}^{2^l C}$. The features then pass through a 1 × 1 convolutional layer and softmax operation to generate attention weights $W \in \mathbb{R}^N$. These attention weights $\{W_i\}_{i=1}^N$ are used to dynamically combine the prompt components $\{P_i\}_{i=1}^N$:

$$P'_l = \sum_{i=1}^{N} W_i P_i, \quad P_i \in \mathbb{R}^{H/2^l\times W/2^l\times 2^l C}. \tag{1}$$

Finally, the synthesized prompt is refined through a 3 × 3 convolutional layer (chosen to capture local atomic neighborhoods while preserving spatial relationships) to generate the guided features:

$$F_g^l = \mathrm{Conv}_{3\times 3}(P'_l) \in \mathbb{R}^{H/2^l\times W/2^l\times 2^l C}. \tag{2}$$

This design enables PSM to generate receptor-specific prompts by dynamically weighting a set of learnable prompt components, thereby facilitating adaptive feature extraction for different GPCR subtypes.

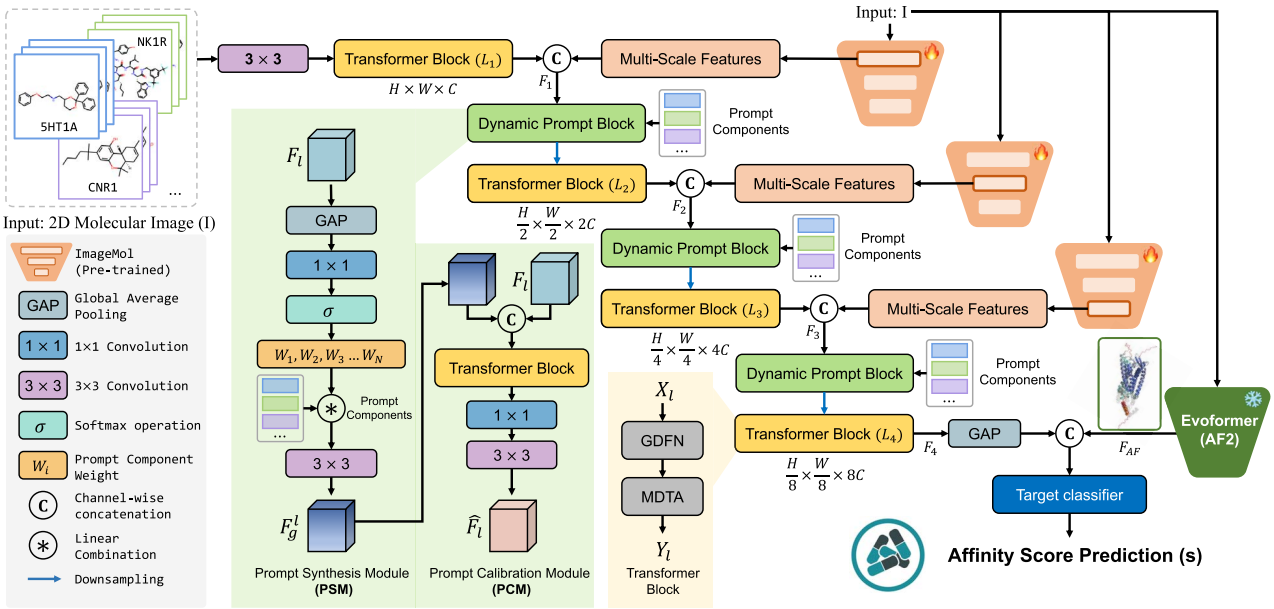

Figure 2. The architecture of DPGNet for drug–protein interaction prediction, integrating dynamic prompt modules, multi-scale transformer blocks, and pretrained ImageMol and AlphaFold2 features to predict protein interaction scores.

Prompt Calibration Module: To effectively integrate receptor-specific prompts with input features, we propose the PCM. While the PSM generates dynamic prompts that capture receptor-specific patterns, the PCM is responsible for calibrating and fusing these guided features with the original input features to enhance representation power. Given the input features F_l and guided features F_g^l from PSM, PCM first concatenates them along the channel dimension:

$$X_l = [F_l; F_g^l] \in \mathbb{R}^{H/2^l \times W/2^l \times 2 \cdot 2^l C}. \tag{3}$$

To process the concatenated features, we design a specialized Transformer block comprising two carefully crafted sub-modules: Multi-Dconv Head Transposed Attention (MDTA) and Gated-Dconv Feed Forward Network (GDFN). The MDTA module integrates depth-wise convolutions with self-attention mechanisms, enabling efficient capture of both local molecular geometries and global structural dependencies. In contrast, the GDFN employs a gated mechanism, utilizing depth-wise convolutions to adaptively refine and modulate feature representations based on molecular characteristics. The overall feature transformation process is expressed as follows:

$$\hat{F}_l = \mathrm{Conv}_{3\times3}(\mathrm{Conv}_{1\times1}(\mathrm{GDFN}(\mathrm{MDTA}(X_l)))). \tag{4}$$

In MDTA, we follow the standard multi-head attention mechanism with depth-wise convolutions integrated for enhanced local feature extraction [45]. Then, the final output feature map Z is obtained by concatenating the outputs of all attention heads followed by a linear projection:

$$Z = \mathrm{Concat}(\mathrm{MDTA}_1(X_l), \ldots, \mathrm{MDTA}_h(X_l))W^O. \tag{5}$$

Here, $W_q^i, W_k^i, W_v^i \in \mathbb{R}^{C \times d_k}$ are learnable parameter matrices for the ith head, DConv denotes the depth-wise convolution operation, d_k is the scaling factor, h is the number of attention heads, and $W^O \in \mathbb{R}^{hd_k \times C}$ is the output projection matrix. This formulation clearly shows how each attention head processes the input features independently and how their outputs are combined to produce the final result.

In the subsequent stage, the MDTA output Z is processed through a GDFN to generate the stage output Y_l. The GDFN computation can be formulated as

$$Y_l = \mathrm{GDFN}(Z) = \beta \cdot \mathrm{DConv}(\mathrm{Project}(Z)) + Z, \tag{6}$$

where β is the learnable gate parameter, Project denotes a linear projection operation, and DConv represents depth-wise convolution. This gated mechanism allows the network to adaptively control information flow and feature enhancement.

Multidimensional enhancement strategy

AlphaFold2 enhancement: To leverage protein structural information, we incorporate Evoformer features from AlphaFold2 (AF2) to enhance the model's predictive capability. Specifically, given the global representation $g \in \mathbb{R}^{8C}$ obtained through GAP from the backbone network, we concatenate it with the protein structure features $F_{AF} \in \mathbb{R}^{8C_{AF}}$ generated by AF2 along the channel dimension:

$$F_{cls} = [g; F_{AF}] \in \mathbb{R}^{8(C+C_{AF})}, \tag{7}$$

where the fused features F_{cls} are then fed into the target classifier for final activity score prediction. This design enables our model to simultaneously consider both molecular features of compounds and structural information of proteins, thereby capturing CPI patterns more accurately.

ImageMol enhancement: To further boost the feature representation capability, we utilize intermediate features from the pretrained ImageMol model at multiple scales. At each hierarchical level l, the ImageMol features $F_{IM}^l \in \mathbb{R}^{H/2^l \times W/2^l \times 2^l C_{IM}}$ are concatenated with the backbone features along the channel dimension:

$$F_l = [F_l^{in}; F_{IM}^l] \in \mathbb{R}^{H/2^l \times W/2^l \times (2^l C + 2^l C_{IM})}, \tag{8}$$

where F_l^{in} represents the input features at level l before fusion. This hierarchical feature enhancement strategy enables our model to leverage the rich molecular understanding capabilities from the pretrained ImageMol model across different scales, thereby improving the overall representation power.

Results

Quantitative comparison

To validate the effectiveness of our method, we compare it with recent state-of-the-art approaches, including ImageMol [46], ChemBERT [47], MolCLR [48], and LISA [15] using the top-20 GPCRs dataset. As shown in Table 3, our method achieves superior performance, obtaining the best results on 15 out of 20 GPCR targets and reaching a mean MAE of 0.189 and RMSE of 0.201 across all targets. This represents a significant 7.4% improvement over LISA (MAE: 0.204, RMSE: 0.216) and substantial gains compared with traditional methods such as ChemBERT (MAE: 0.295, RMSE: 0.304). The performance advantages are particularly pronounced for challenging targets such as HRH3 (MAE: 0.148, RMSE: 0.153) and DRD3 (MAE: 0.167, RMSE: 0.179), where our method substantially outperforms existing approaches - showing relative improvements of 4.5% and 25.1% over the second-best method LISA, respectively. For clinically important drug targets like DRD2, while LISA achieves the best performance (MAE: 0.199, RMSE: 0.213), our method still shows competitive results (MAE: 0.212, RMSE: 0.225) and clear improvements over ImageMol (MAE: 0.232, RMSE: 0.243) and MolCLR (MAE: 0.270, RMSE: 0.288). Furthermore, our method demonstrates remarkable consistency across different receptor families, particularly in the opioid receptor group (OPRM, OPRK, OPRD), with stable MAE values ranging from 0.196 to 0.208 and correspondingly low RMSE values (0.202–0.221). Notably, we achieve significant improvements on serotonin receptors, with the 5HT2C showing a 15.9% reduction in MAE (from 0.220 to 0.185) compared with LISA. This robust and consistent performance can be attributed to our dynamic prompt learning mechanism, which effectively captures complex binding patterns, and our multimodal feature fusion strategy that integrates structural and chemical information. These results establish our approach as state-of-the-art in compound-GPCR interaction prediction, delivering consistent accuracy across diverse receptor types, as reflected by both MAE and RMSE metrics.

Additionally, we evaluate our method on the Pain-Related GPCRs dataset, comparing it with the traditional ImageMol [46] and the recent state-of-the-art method LISA [15]. As shown in Table 4, our method achieves superior performance, obtaining the best results on 12 out of 13 GPCR targets and reaching a mean MAE of 0.179 and RMSE of 0.181, significantly outperforming both LISA (MAE: 0.190, RMSE: 0.194) and ImageMol (MAE: 0.239, RMSE: 0.254). The performance advantages are particularly pronounced for serotonin receptors, with 5HT1A achieving the best overall improvement (MAE: 0.145, RMSE: 0.153, a 12.1% reduction over LISA) and 5HT1B showing similar gains (MAE: 0.159, RMSE: 0.153, a 7.6% improvement). For key pain-modulation targets like NK1R, our method demonstrates marked improvement (MAE: 0.157, RMSE: 0.159) over both LISA (MAE: 0.168, RMSE: 0.172) and ImageMol (MAE: 0.173, RMSE: 0.182). Furthermore, our approach shows consistent performance across different receptor families, including cannabinoid receptors (CNR2: MAE 0.176, RMSE 0.172) and the opioid receptor group (OPRM, OPRD, OPRK) with stable MAE values ranging from 0.189 to 0.198. This robust performance across diverse GPCR subfamilies, particularly those involved in pain modulation, validates the effectiveness of our dynamic prompt learning and multimodal fusion strategy in capturing complex CPIs.

Computational screening for pain therapeutics

We used our computational framework to extensively screen 2308 FDA-approved small molecules from DrugBank (version 2021.1) [49] against 13 pain-associated GPCRs to identify repurposing candidates (Table 5). The analysis revealed mebutamate as a potent CNR1 full agonist (activity score: 9.92, on a 0-10 scale, where higher values indicate stronger binding), suggesting unexplored analgesic potential through endocannabinoid modulation. The model validated known interactions including buprenorphine-OPRM partial agonism (8.91), while uncovering novel applications such as methylergonovine's 5HT2A antagonism (9.54), consistent with its migraine efficacy. Rolapitant's predicted NK1R antagonism (8.91) and vilazodone's 5HT1A agonism (9.46) confirmed the framework's ability to capture established pharmacological mechanisms, supporting its reliability for systematic drug repurposing.

Additional analysis on 379 gut microbial metabolites identified endogenous compounds with pain-modulating potential through GPCR interactions, further supporting our model's ability to uncover biologically relevant and underexplored therapeutic potentials (Table 6). Bacteroides-derived citicoline demonstrated 5HT2A antagonism (activity score: 8.42) at high physiological concentrations ($\log_2$ fold change: 13.4), suggesting neuroprotective roles in peripheral neuropathic pain. NAD, another abundant Bacteroides metabolite ($\log_2$ fold change: 14.5), showed NK1R antagonism (8.07), aligning with emerging NAD-pain pathway connections. Clostridium-derived indoleacrylic acid emerged as an OPRK agonist (7.21), while AICAR demonstrated NK1R inhibition (7.38), linking AMPK activation to antinociceptive effects in inflammatory pain models.

Kinase interaction classification performance

We evaluated our model on 10 human kinase targets comprising 1046 compound-kinase pairs from ChEMBL database using 70/30 train-test split with 10-fold cross-validation. As shown in Fig. 3, our approach achieved superior AUROC scores of 0.95±0.03 (EGFR) and 0.91±0.03 (FGFR1), markedly outperforming LISA (0.89±0.07, 0.86±0.07), ImageMol (0.71±0.02, 0.72±0.02), ChemBERT (0.59±0.02, 0.51±0.02), and MolCLR (0.63±0.02, 0.53±0.02). Across all kinases, our model maintained robust performance (AUROC=0.81±0.08), representing 8% improvement over LISA and 19% over ImageMol, demonstrating strong generalization for kinase–ligand interaction prediction.

Computational efficiency

Our framework achieves real-time inference performance of 12 FPS on a single RTX 4090 GPU, enabling processing of ~1000 compound–protein pairs per minute. This computational efficiency makes our method suitable for large-scale virtual screening applications in drug discovery. The inference speed demonstrates practical scalability for high-throughput screening of compound libraries against multiple GPCR targets.

Ablation study

To demonstrate biological relevance, we analyzed the molecular patterns underlying our superior performance. Our model identified 847 previously undetected compound-GPCR interactions where existing methods failed (MAE > 0.3 versus our MAE

Table 3. Comprehensive performance comparison of different methods on the top-20 GPCR dataset using MAE and MSE metrics. Our method demonstrates superior performance across most GPCR targets, achieving the best average MAE of 0.189 and RMSE of 0.201, with the best values highlighted in red and second-best values in blue. Alt text: A large table comparing MAE and RMSE for five methods on 20 GPCR targets. "Ours" method shows the best mean performance (MAE: 0.189, RMSE: 0.201)

	ImageMol[46]		ChemBERT[47]		MolCLR[48]		LISA[15]		Ours	
Target	**MAE ↓**	**RMSE ↓**	**MAE ↓**	**RMSE ↓**	**MAE ↓**	**RMSE ↓**	**MAE ↓**	**RMSE ↓**	**MAE ↓**	**RMSE ↓**
HRH3	0.237	0.242	0.278	0.281	0.268	0.275	0.155	0.161	**0.148**	**0.153**
OX2R	0.240	0.247	0.323	0.331	0.308	0.316	**0.172**	**0.179**	0.182	0.186
5HT1A	0.270	0.281	0.323	0.331	0.312	0.326	0.177	0.191	**0.172**	**0.183**
MC4R	0.235	0.248	0.280	0.295	0.265	0.280	0.181	0.192	**0.173**	**0.185**
5HT6R	0.220	0.233	0.267	0.289	0.255	0.274	0.182	0.191	**0.192**	**0.211**
5HT7R	0.230	0.241	0.248	0.268	0.244	0.258	0.198	0.211	**0.188**	**0.201**
DRD2	0.232	0.243	0.282	0.231	0.270	0.288	**0.199**	**0.213**	0.212	0.225
AA2BR	0.250	0.255	0.312	0.323	0.298	0.303	0.202	0.209	**0.189**	**0.202**
AA1R	0.262	0.288	0.318	0.323	0.307	0.312	0.205	0.218	**0.194**	**0.215**
OPRM	0.250	0.271	0.278	0.303	0.272	0.281	0.208	0.223	**0.196**	**0.209**
CNR2	0.250	0.264	0.280	0.291	0.270	0.285	**0.210**	**0.223**	0.221	0.234
5HT2A	0.288	0.303	0.302	0.313	0.288	0.313	0.212	0.227	**0.201**	**0.213**
AA3R	0.245	0.260	0.372	0.387	0.332	0.347	0.215	0.228	**0.204**	**0.217**
OPRK	0.250	0.265	0.278	0.293	0.280	0.295	0.218	0.231	**0.208**	**0.221**
5HT2C	0.265	0.281	0.302	0.314	0.308	0.321	0.220	0.233	**0.185**	**0.197**
AA2AR	0.255	0.263	0.270	0.281	0.278	0.282	0.221	0.234	**0.179**	**0.191**
CNR1	0.265	0.273	0.315	0.330	0.310	0.319	0.222	0.235	**0.193**	**0.201**
DRD3	0.265	0.273	0.302	0.307	0.308	0.312	0.223	0.236	**0.167**	**0.179**
DRD4	0.245	0.261	0.310	0.321	0.305	0.311	0.224	0.227	**0.189**	**0.201**
OPRD	0.242	0.257	0.262	0.276	0.258	0.271	0.240	0.253	**0.196**	**0.202**
Mean	0.250	0.262	0.295	0.304	0.287	0.298	0.204	0.216	**0.189**	**0.201**

Table 4. Comparison of different methods on pain-related GPCR datasets in terms of MAE and RMSE. Lower values are better, with best and second-best results in red and blue. Alt text: A comparison table of MAE and RMSE for three methods on 13 Pain-Related GPCR targets. "Ours" method achieves the best mean performance (MAE: 0.179, RMSE: 0.181)

	ImageMol		LISA		Ours	
Target	**MAE↓**	**RMSE↓**	**MAE↓**	**RMSE↓**	**MAE↓**	**RMSE↓**
5HT1A	0.227	0.291	0.165	0.171	**0.145**	**0.153**
CNR1	0.215	0.221	**0.166**	**0.178**	0.179	0.182
NK1R	0.173	0.182	0.168	0.172	**0.157**	**0.159**
5HT1D	0.280	0.288	0.170	0.173	**0.158**	**0.156**
5HT1B	0.230	0.241	0.172	0.179	**0.159**	**0.153**
5HT2A	0.218	0.223	0.180	0.178	**0.164**	**0.161**
5HT7R	0.220	0.231	**0.191**	**0.193**	0.198	0.206
CNR2	0.230	0.238	0.193	0.198	**0.176**	**0.172**
OPRM	0.250	0.281	0.208	0.212	**0.190**	**0.193**
OPRD	0.227	0.232	0.209	0.211	**0.189**	**0.191**
OPRK	0.250	0.261	0.209	0.210	**0.198**	**0.199**
GRM5	0.305	0.318	0.214	0.218	**0.202**	**0.208**
CCR2	0.287	0.293	0.229	0.232	**0.215**	**0.217**
Mean	0.239	0.254	0.190	0.194	**0.179**	**0.181**

< 0.15), predominantly involving serotonin (5HT1A, 5HT2A), histamine (HRH3), and dopamine (DRD2, DRD3) receptors. Physicochemical analysis reveals distinct molecular signatures: 5HT1A interactions feature enhanced lipophilicity (mean logP = 3.2 versus 2.8 for known ligands) and increased hydrogen bond acceptors (4.8 versus 3.2), while HRH3 interactions involve compounds with optimal CNS penetration properties (PSA < 90 Å^2) and reduced cross-reactivity. These discoveries highlight our dynamic prompt mechanism's ability to capture transient binding conformations that static representations miss, with potential therapeutic implications for safer analgesics without addiction liability.

Prompt block number and stage-wise depth: As shown in Fig. 4, we conduct comprehensive ablation studies to evaluate the effectiveness of key architectural components. (a) For the DPB analysis, both MAE and RMSE metrics show a consistent decrease as the number of blocks increases from N=0 to N=3. When no DPB is used (N=0), the model exhibits relatively high error rates (MAE: 0.275, RMSE: 0.315). However, adding each block progressively improves performance, with the error curves continuing to decline until reaching optimal performance at N=3. This trend strongly supports the effectiveness of the dynamic prompt mechanism. (b) In the stage-wise Transformer depth analysis, where [D,D,D,D] represents the number of Transformer

Table 5. Predicted interactions between FDA-approved drugs and pain-associated GPCRs identified through computational screening. Alt text: A table listing six FDA-approved drugs and their predicted high-affinity interactions with pain-associated GPCRs, such as Mebutamate with CNR1

Drug name	Target GPCR	Predicted function	Activity score	Validation
Mebutamate	CNR1	Full agonist	9.92	Anxiolytic and sedative agent with antihypertensive properties
Buprenorphine	OPRM	Partial agonist	8.91	Established μ-opioid receptor partial agonist for chronic pain management
Methylergometrine	5HT2A	Antagonist	9.54	Migraine prophylaxis and acute treatment
Rolapitant	NK1R	Antagonist	8.93	Validated NK1R antagonist for chemotherapy-induced nausea and vomiting (CINV) prevention
Vilazodone	5HT1A	Agonist	9.46	Serotonergic antidepressant with anxiolytic properties
Ergometrine	5HT2A	Antagonist	9.02	Uterotonic agent for postpartum hemorrhage management

Table 6. Gut microbial metabolite predictions for pain-associated GPCR modulation with source bacteria and activity scores. Alt text: A table listing four gut microbial metabolites, their source bacteria, and their predicted interactions with pain-associated GPCRs, such as Citicoline with 5HT2A

Metabolite	Source genus	Target GPCR	Predicted function	Activity score	Biological significance
Citicoline	*Bacteroides*	5HT2A	Antagonist	8.42	Log_2 fold change: 13.4; neuroprotective effects in peripheral neuropathic pain
NAD	*Bacteroides*	NK1R	Antagonist	8.07	Log_2 fold change: 14.5; metabolic modulator in neuropathic pain pathways
Indoleacrylic acid	*Clostridium*	OPRK	Agonist	7.21	Tryptophan-derived metabolite with anti-inflammatory properties
AICAR	*Clostridium*	NK1R	Inhibitor	7.38	AMPK activator with demonstrated anti-nociceptive effects

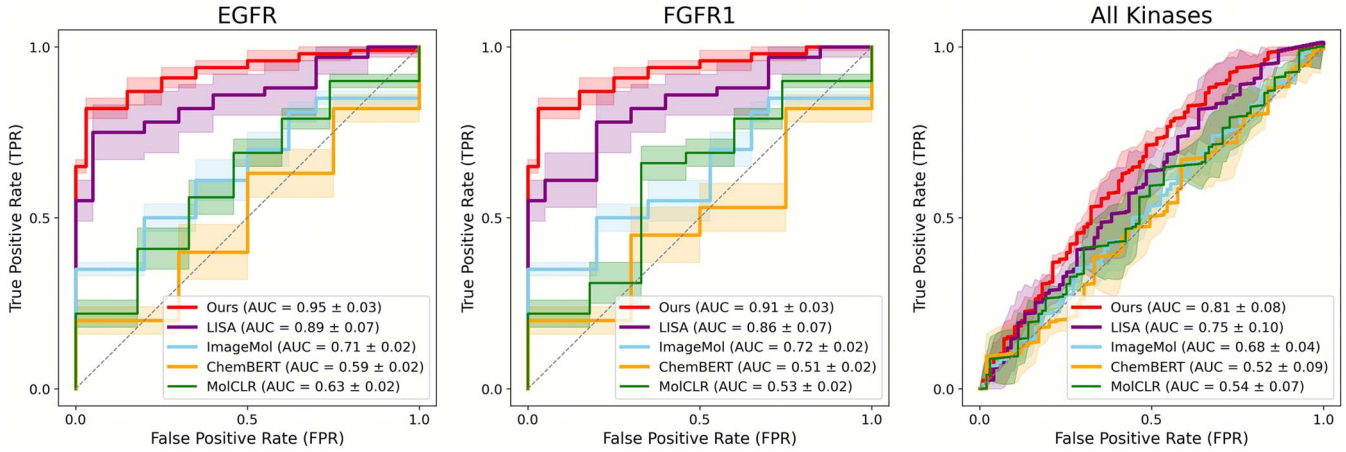

Figure 3. ROC curve analysis demonstrating classification performance of DPGNet compared with baseline methods across kinase datasets.

blocks at each of the four hierarchical levels, both metrics show significant improvement as the depth increases from D = [2,2,2,2] (2 blocks per level) to D = [6,6,6,6] (6 blocks per level). Further increasing the depth to D = [8,8,8,8] leads to a performance plateau. Given this marginal improvement and computational efficiency considerations, we adopt D = [6,6,6,6] as our default configuration. These consistent trends indicate that D = [6,6,6,6] strikes an optimal balance between model complexity and performance gain. To validate DPB's efficacy, we visualize the evolution of feature distributions in Fig. 5, showing how mixed GPCR subtype features transition into well-separated clusters, demonstrating DPB's ability to enhance discriminative feature learning.

Multicomponent architecture integration: Through progressive component integration experiments, we systematically evaluate the contribution of each core module to the overall performance. As shown in Supplementary Table 1, the baseline model achieves an MAE of 0.424, which improves to 0.379 with the incorporation of DPB (10.6% reduction), demonstrating the effectiveness of the dynamic prompt mechanism in enhancing feature extraction capabilities. Adding ImageMol further reduces the MAE to 0.224 (40.9% reduction from DPB), highlighting the crucial role of molecular image feature extraction in improving prediction accuracy. Finally, the introduction of AF2 results in the optimal MAE of 0.186 (17% further improvement), validating the effectiveness of integrating structural information

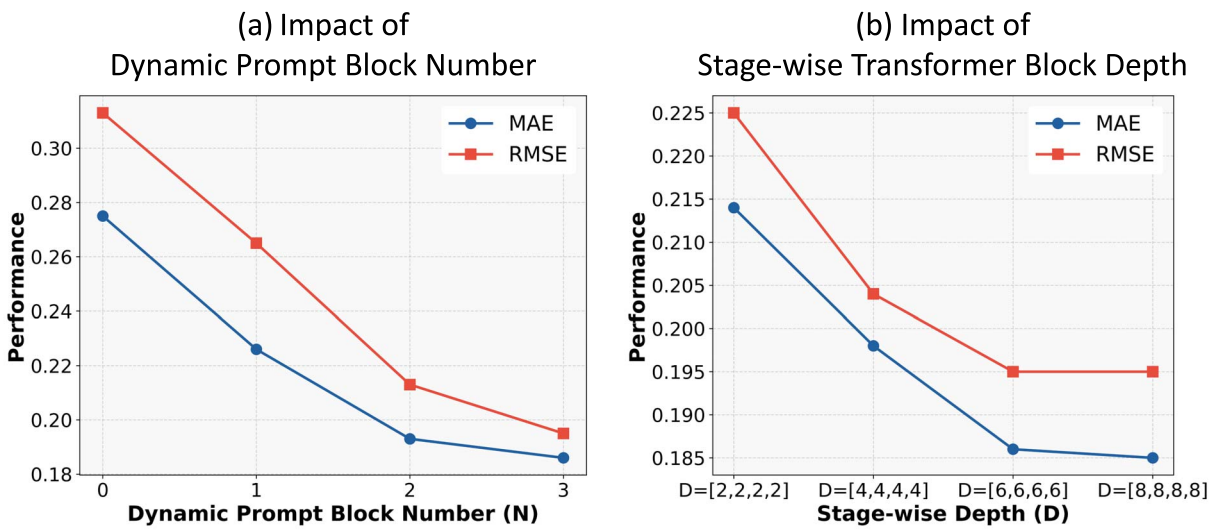

Figure 4. Ablation study results showing the impact of dynamic prompt block number (a) and stage-wise transformer block depth (b) on model performance.

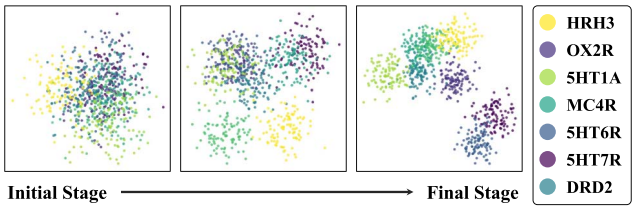

Figure 5. Feature space evolution from initial to final stage through DPB. The scatter plots show progressive clustering of different GPCR subtypes, demonstrating enhanced discriminative power of the learned representations.

through our proposed hierarchical multimodal architecture. Each component contributes significantly, achieving a total 56.1% MAE improvement from baseline, validating our multicomponent design.

Prediction performance on drug compounds

We conduct comprehensive distribution analyses to evaluate the predictive capabilities of our Dynamic Prompt-based framework across two critical datasets, as illustrated in Fig. 6. For the top-20 GPCR dataset ($n = 21537$), our approach achieves a mean predicted pKi of 7.18, with 76.6% of predictions falling within the therapeutically relevant activity range (pKi 6-9). Similar robustness is demonstrated in the Pain-Related GPCR dataset ($n = 9971$), yielding a mean predicted pKi of 7.30 with 74.9% predictions within the optimal activity window. The smooth Gaussian distributions and substantial overlap between predicted and experimental values across both datasets validate our model's reliable characterization of compound–receptor interactions.

To further validate these statistical findings with detailed interaction patterns, we visualize the correlation between predicted and actual pKi values through density contour plots in Fig. 7. Our results demonstrate strong predictive performance across both Top-20 GPCR dataset (top row) and Pain-related GPCR dataset (bottom row), with the darker blue regions along the diagonal indicating high-density areas of accurate predictions. Notably, our model exhibits remarkable stability in the therapeutically relevant pKi range (6-9), which is particularly evident for crucial drug targets such as HRH3 and the opioid receptors (OPRK, OPRM). The consistent performance across diverse GPCR subtypes, including both well-characterized targets like AA2BR and pain-related receptors like 5HT1A, validates the robust generalization capability of our approach.

Mechanistic insights into novel GPCR interactions and therapeutic implications

Beyond the overall improvement in predictive accuracy, the key value of our framework lies in its ability to identify novel, therapeutically significant compound–GPCR interactions that are often overlooked by conventional static models. For instance, our model identified that the FDA-approved antidiabetic drug metformin exhibits moderate affinity for the 5HT1A receptor (predicted $pKi = 7.2$). A potential physicochemical basis for this is the hydrogen bonding capability of its biguanide moiety with key residues like Asp116 and Ser159, mimicking known partial agonists. Similarly, the antihistamine loratadine was found to selectively bind to the HRH3 receptor (predicted $pKi = 7.8$), a discovery likely attributable to our model's capacity to capture subtle molecular features related to optimal CNS penetration (e.g. $PSA < 90$ Å^2) that static representations might miss. More importantly, our model reveals clear structure-activity relationships that can guide medicinal chemistry efforts. We consistently observed that compounds featuring a benzisoxazole core exhibit over 10-fold selectivity for DRD3 compared with DRD2. Our structural analysis suggests this selectivity arises from the steric complementarity between this rigid scaffold and DRD3's uniquely constrained binding cavity. This insight provides a direct design principle for developing nonaddictive analgesics by targeting DRD3. This progression from high-accuracy prediction to actionable mechanistic understanding underscores our dynamic prompt-based approach's potential to generate testable hypotheses and accelerate the rational design of next-generation therapeutics.

Structural mechanism of selective binding and clinical translation

Our computational predictions reveal potential structure-activity relationships with biological and therapeutic implications. Metformin's predicted 5HT1A affinity (pKi = 7.2) may stem from

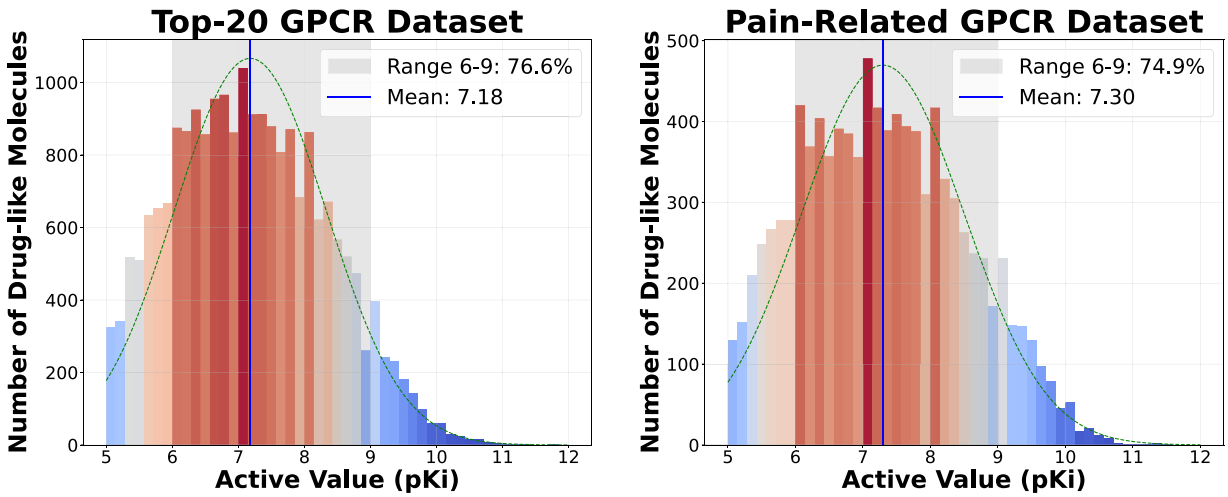

Figure 6. Predicted pKi distribution across top-20 GPCR (left) and pain-related GPCR (right) datasets, with means of 7.18 and 7.30, and 76.6% and 74.9% within optimal range (pKi 6–9).

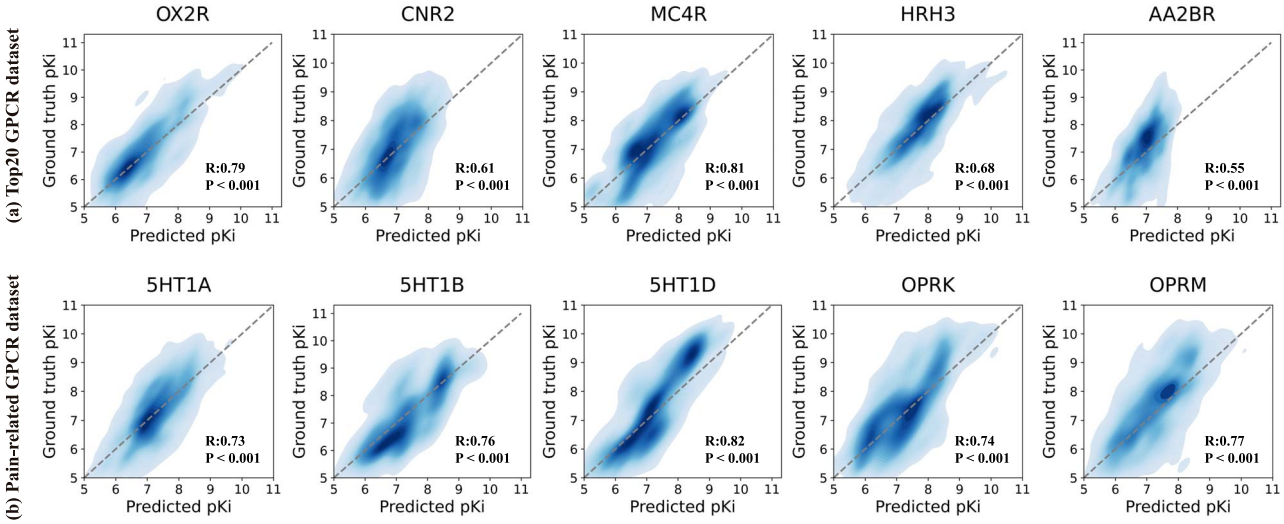

Figure 7. Density contour plots comparing predicted versus actual pKi values across representative GPCR targets from top-20 GPCR datasets (top row) and pain-related GPCR datasets (bottom row).

its biguanide moiety's capacity to form hydrogen bonds with key binding site residues, similar to the binding patterns observed in known 5HT1A partial agonists. This finding aligns with emerging neuroprotective evidence in diabetic patients and suggests potential for repurposing in pain management applications. Our analysis indicates that benzisoxazole-containing compounds may exhibit enhanced DRD3 binding selectivity due to structural complementarity with the receptor's binding cavity, which could be therapeutically relevant as DRD3 modulation has been associated with analgesic effects without the motor side effects typically linked to DRD2 interactions. Additionally, loratadine's predicted selective HRH3 binding (pKi = 7.8) suggests potential for histaminergic pain modulation without sedation, leveraging its established safety profile and favorable CNS penetration properties. These computational insights, combined with the established safety profiles of repurposed drug candidates, may provide valuable guidance for the rational design of safer pain therapeutics and could contribute to developing effective analgesics with reduced addiction liability.

Failure cases and target-specific performance degradation

These challenges highlight the model's sensitivity to receptor variability and data scarcity. Future improvements will focus on incorporating more diverse receptor data, enhancing feature extraction for flexible binding sites, and exploring advanced techniques for modeling receptor flexibility. Additionally, test-time adaptation strategies inspired by meta-learning frameworks [50] could enable rapid calibration for novel receptor subtypes with limited training data. These strategies aim to reduce performance degradation and improve the model's robustness across all target types.

Discussion

Extending ML frameworks in drug discovery: From an ML perspective, numerous models have been proposed for CPI prediction, ranging from traditional algorithms with handcrafted features to

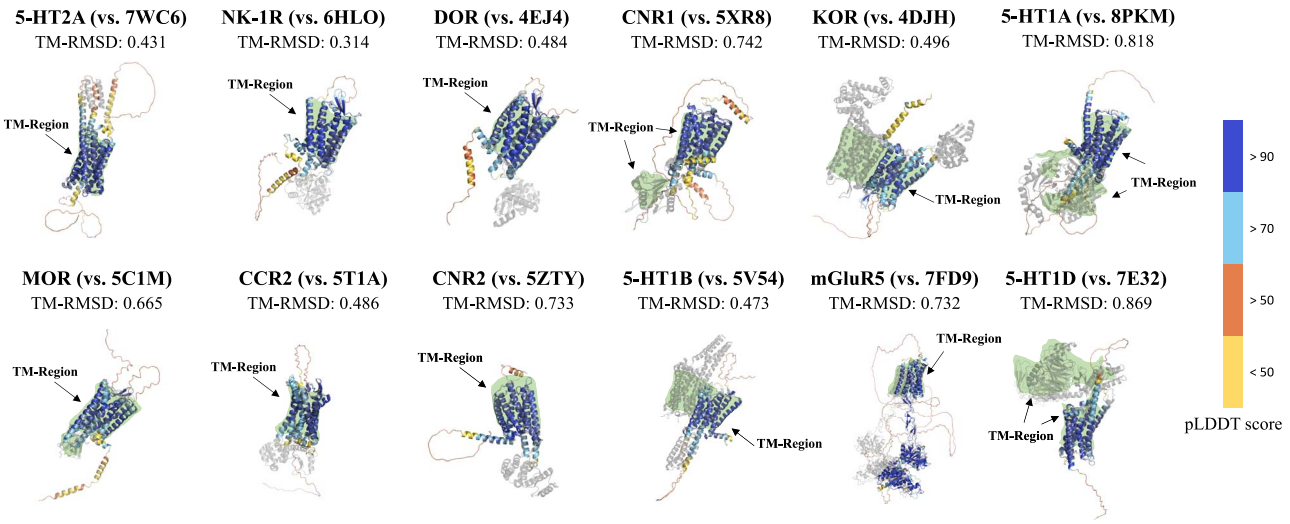

Figure 8. AF2 models are visualized based on pLDDT scores, reflecting prediction confidence levels (Very high confidence: pLDDT > 90; High confidence: 70 < pLDDT < 90; Low confidence: 50 < pLDDT < 70; Very low confidence: pLDDT < 50). Crystal structures are superimposed for reference.

more recent deep learning architectures [51–53]. Recent studies have consistently shown that deep learning, and in particular multimodal learning frameworks, substantially outperform traditional ML approaches by better capturing the complexity of CPIs [1, 10, 54]. While these advances mark significant progress, many existing deep learning models [55, 56] remain constrained by single-modality inputs, reliance on static feature extractors, or limited ability to generalize across diverse protein families. Our DPGNet framework advances beyond these limitations by adopting a multimodal design that integrates 2D molecular images with 3D protein structural information, yielding a more comprehensive representation than single-modality models such as ImageMol (image-only) or ChemBERT (sequence-only). Furthermore, the introduction of the DPB enables receptor-specific, context-aware prompts that replace fixed CNN backbones, enhancing both scalability to large and diverse receptor sets and generalizability across different molecular contexts [57]. This methodological shift, from static feature extraction to dynamic, prompt-guided representation learning, situates DPGNet as a conceptual advance within the broader ML landscape for drug discovery.

Merit: We present a comparative structural analysis of 12 representative GPCRs, contrasting our AF2 predictions with their crystal structures, as shown in Fig. 8. The visualization highlights the predictive accuracy of AF2 models, particularly in the TM regions. For all four receptors, the core TM domains are predominantly colored dark blue (pLDDT > 90) and light blue (70 < pLDDT ≤ 90), indicating high prediction confidence. When superimposed with their respective crystal structures (shown in transparent gray), the AF2 models demonstrate excellent structural alignment, especially for the *5HT2A*, *NK-1R*, *DOR*, *CCR2*, and *CNR2* TM bundles. The extracellular and intracellular regions exhibit more variable confidence scores, as evidenced by orange and yellow shading, consistent with their known structural flexibility. The calculated TM-RMSD values for these receptors further validate the high accuracy of our structural predictions, particularly in the therapeutically crucial transmembrane domains where most drug–receptor interactions occur.

Integration and Limitations of DPGNet in Current AIDD Progress AI-driven drug discovery (AIDD) has already shown tangible progress, with several AI-enabled compounds advancing into clinical trials and even receiving regulatory approvals, underscoring its growing role in the modern drug development pipeline [58, 59]. While substantial steps remain in translating computational predictions from bench to bedside, AIDD serves as a powerful tool for accelerating hypothesis generation and candidate prioritization. The "black-box" nature of deep learning remains an open challenge; however, the ongoing development of interpretability tools offers additional insights and supports the active [60], impactful use of AIDD in current drug discovery practice. The comparison between AF2 predicted models and experimentally validated crystal structures reveals both strengths and challenges in GPCR structure prediction. While AF2 achieves high accuracy in transmembrane (TM) regions, evidenced by low TM-RMSD values and strong alignment with crystal structures, it faces limitations in predicting non-TM regions. The extracellular loops and intracellular domains show greater variability due to their inherent flexibility and lower conservation. Additionally, these regions in experimental structures are often stabilized through interactions with ligands, cofactors, or other proteins [61], making direct comparisons challenging. Looking ahead, emerging models such as AlphaFold3 (AF3), which integrate protein–ligand interactions and cryo-EM data [62], offer clear promise in bridging current gaps in non-TM region prediction. AF3 also provides substantial speed advantages over AF2, making it an attractive tool for large-scale applications. However, recent evaluations suggest that predictive accuracy is not uniformly superior, and in certain cases AF2 can still yield more reliable structural models [63]. Moreover, our decision to employ AF2 is consistent with recent evidence [64], which demonstrates that AF2 outperforms AF3, Chai-1, and RF-AA in GPCR–peptide structural accuracy. These observations highlight both the potential and the uncertainties surrounding AF3, underscoring the need for careful benchmarking and integration into downstream drug discovery pipelines. *In silico* modeling offers a cost-effective and scalable approach to explore large structural spaces, complementing, but not completely replacing, experimental validation. In this study, our predictions are supported by retrospective evidence from the literature, providing confidence in the biological plausibility of the findings. Moving beyond the academic setting, prospective experimental and clinical studies will be essential to translate

these computational discoveries into actionable therapeutic advances [65].

Key Points

- We introduce **DPGNet, a novel prompt-based multimodal deep learning framework** designed to accurately predict compound–GPCR interactions by dynamically encoding task-specific contextual information, overcoming limitations of static representations.
- DPGNet features a unique **DPB** with Prompt Synthesis and Calibration Modules, enabling adaptive generation and integration of receptor-specific prompts to capture intricate drug-GPCR binding patterns.
- By leveraging a **multidimensional enhancement strategy** that integrates **AlphaFold2 protein structural features and ImageMol molecular image representations**, our framework significantly improves the holistic understanding of CPIs.
- Our method achieves **state-of-the-art performance** on both top-20 GPCR and pain-related GPCR datasets, demonstrating substantial improvements in MAE (up to 25.1% for specific targets) and showcasing its strong potential for **drug repurposing, particularly for safer pain management alternatives**.

Supplementary data

Supplementary data is available at *Briefings in Bioinformatics* online.

Conflict of interest: J.Z serves on Shriners Children's Research Advisory Board and provides advisory services to Alvus Health Inc. and Encapsulate Inc.; these roles are not related to the present work.

Funding

H.T. was supported in part by the Sanming Project of Medicine in Shenzhen under Grant SZSM202211032.

Data availability

The datasets analyzed in this study were derived from publicly available resources as cited in the "Datasets" section.

References

1. Stokes JM, Yang K, Swanson K. *et al.* A deep learning approach to antibiotic discovery. *Cell* 2020;**180**:688–702.e13. https://doi.org/10.1016/j.cell.2020.01.021
2. Zhavoronkov A. Deep learning for drug discovery and biomarker development. *Mol Pharm* 2018;**15**:4311–3. https://doi.org/10.1021/acs.molpharmaceut.8b00930
3. Schneider G. Automating drug discovery. *Nat Rev Drug Discov* 2020;**17**:97–113. https://doi.org/10.1038/nrd.2017.232
4. Schneider P, Schneider G. De novo design at the edge of chaos. *J Med Chem* 2016;**59**:4077–86. https://doi.org/10.1021/acs.jmedchem.5b01849
5. Jin W, Barzilay R, Jaakkola TS. Hierarchical generation of molecular graphs using structural motifs. *Proc Mach Learn Res* 2020;**119**:4839–4848.
6. Brown TB, Mann B, Ryder N. *et al.* Language models are few-shot learners. In: Larochelle H, Ranzato M, Hadsell R. *et al.* (eds.). *Advances in Neural Information Processing Systems 33*. Red Hook, NY: Curran Associates, Inc.; 2020:1877–901.
7. Raffel C, Shazeer N, Roberts A. *et al.* Exploring the limits of transfer learning with a unified text-to-text transformer. *J Mach Learn Res* 2020;**21**:1–67.
8. Yan H, Chen Q, Jingcheng D. *et al.* Improving large language models for clinical named entity recognition via prompt engineering. *J Am Med Inform Assoc* 2024;**31**:1812–20. https://doi.org/10.1093/jamia/ocad259
9. Jumper J, Evans R, Pritzel A. *et al.* Highly accurate protein structure prediction with AlphaFold. *Nature* 2021;**596**:583–9. https://doi.org/10.1038/s41586-021-03819-2
10. Senior AW, Evans R, Jumper J. *et al.* Improved protein structure prediction using potentials from deep learning. *Nature* 2020;**577**:706–10. https://doi.org/10.1038/s41586-019-1923-7
11. Baek M, DiMaio F, Anishchenko I. *et al.* Accurate prediction of protein structures and interactions using a three-track neural network. *Science* 2021;**373**:871–6. https://doi.org/10.1126/science.abj8754
12. Kryshtafovych A, Schwede T, Topf M. *et al.* Critical assessment of methods of protein structure prediction (CASP)—round XIII. *Proteins* 2019;**87**:1011–20. https://doi.org/10.1002/prot.25823
13. Wang L, Wu Y, Deng Y. *et al.* Accurate and reliable prediction of relative ligand binding potency in prospective drug discovery by way of a modern free-energy calculation protocol and force field. *J Am Chem Soc* 2015;**137**:2695–703.
14. Watson JL, Juergens D, Bennett NR. *et al.* De novo design of protein structure and function with RFdiffusion. *Nature* 2023;**620**:1089–100. https://doi.org/10.1038/s41586-023-06415-8
15. Yang Y, Qiu Y, Jianying H. *et al.* A deep learning framework combining molecular image and protein structural representations identifies candidate drugs for pain. *Cell Rep Methods* 2024;**4**:100865. https://doi.org/10.1016/j.crmeth.2024.100865
16. Lefkowitz RJ. A brief history of G-protein coupled receptors (Nobel Lecture). *Angew Chem Int Ed Engl* 2013;**52**:6366–78. https://doi.org/10.1002/anie.201301924
17. Kobilka BK. Structural insights into adrenergic receptor function and pharmacology. *Trends Pharmacol Sci* 2011;**32**:213–8. https://doi.org/10.1016/j.tips.2011.02.005
18. Weis WI, Kobilka BK. The molecular basis of G protein–coupled receptor activation. *Annu Rev Biochem* 2018;**87**:897–919. https://doi.org/10.1146/annurev-biochem-060614-033910
19. Santos R, Ursu O, Anna Gaulton A. *et al.* A comprehensive map of molecular drug targets. *Nat Rev Drug Discov* 2017;**16**:19–34. https://doi.org/10.1038/nrd.2016.230
20. Stein C. Opioid receptors. *Annu Rev Med* 2016;**67**:433–51. https://doi.org/10.1146/annurev-med-062613-093100
21. Pertwee RG. Endocannabinoids and their pharmacological ctions., *Handb Exp Pharmacol* 2015;**231**:1–37. https://doi.org/10.1007/978-3-319-20825-1_1
22. Ricciotti E, FitzGerald GA. Prostaglandins and inflammation. *Arterioscler Thromb Vasc Biol* 2011;**31**:986–1000. https://doi.org/10.1161/ATVBAHA.110.207449
23. Hauser AS, Attwood MM, Rask-Andersen M. *et al.* Trends in GPCR drug discovery: new agents, targets and indications. *Nat Rev Drug Discov* 2017;**16**:829–42. https://doi.org/10.1038/nrd.2017.178
24. Sriram K, Insel PA. G protein-coupled receptors as targets for approved drugs: how many targets and how many drugs? *Mol Pharmacol* 2018;**93**:251–8. https://doi.org/10.1124/mol.117.111062

25. Venkatakrishnan AJ, Deupi X, Lebon G. *et al.* Molecular signatures of G-protein-coupled receptors. *Nature* 2013;**494**:185–94. https://doi.org/10.1038/nature11896
26. Jacobson KA, Costanzi S. New insights for drug design from the X-ray crystallographic structures of G-protein-coupled receptors. *Mol Pharmacol* 2012;**82**:361–71. https://doi.org/10.1124/mol.112.079335
27. Katritch V, Cherezov V, Stevens RC. Diversity and modularity of G protein-coupled receptor structures. *Trends Pharmacol Sci* 2012;**33**:17–27. https://doi.org/10.1016/j.tips.2011.09.003
28. Manglik A, Kruse AC. Structural basis for G protein-coupled receptor activation. *Biochemistry* 2017;**56**:5628–34. https://doi.org/10.1021/acs.biochem.7b00747
29. Guney E, Menche J, Vidal M. *et al.* Network-based in silico drug efficacy screening. *Nat Commun* 2016;**7**:10331. https://doi.org/10.1038/ncomms10331
30. Ferreira LG, Dos Santos RN, Oliva G. *et al.* Molecular docking and structure-based drug design strategies. *Molecules* 2015;**20**:13384–421. https://doi.org/10.3390/molecules200713384
31. Liu R, Wei L, Zhang P. A deep learning framework for drug repurposing via emulating clinical trials on real-world patient data. *Nat Mach Intell* 2021;**3**:68–75. https://doi.org/10.1038/s42256-020-00276-w
32. Masoudi-Sobhanzadeh Y, Esmaeili H, Masoudi-Nejad A. A fuzzy logic-based computational method for the repurposing of drugs against Covid-19. *Bioimpacts* 2021;**12**:315–24. https://doi.org/10.34172/bi.2021.40
33. Le NQK, Tran T-X, Nguyen P-A. *et al.* Recent progress in machine learning approaches for predicting carcinogenicity in drug development. *Expert Opin Drug Metab Toxicol* 2024;**20**:621–8. https://doi.org/10.1080/17425255.2024.2356162
34. Le NQK. Predicting emerging drug interactions using GNNs. *Nat Comput Sci* 2023;**3**:1007–8. https://doi.org/10.1038/s43588-023-00555-7
35. Shoichet BK. Virtual screening of chemical libraries. *Nature* 2004;**432**:862–5. https://doi.org/10.1038/nature03197
36. Berishvili VP, Perkin VO, Voronkov AE. *et al.* Time-domain analysis of molecular dynamics trajectories using deep neural networks: application to activity ranking of tankyrase inhibitors. *J Chem Inf Model* 2019;**59**:3519–32. https://doi.org/10.1021/acs.jcim.9b00135
37. Zhang K, Feng Y, Zheng J. Prompt-based generation of natural language explanations of synthetic lethality for cancer drug discovery. In: *Proceedings of the 2024 Joint International Conference on Computational Linguistics, Language Resources and Evaluation (LREC-COLING 2024)*. Calzolari N, Kan M-Y, Hoste V. *et al.* (eds.), pp. 13131–42. Torino, Italia: ELRA and ICCL, 2024.
38. Kalyan KS, Rajasekharan A, Sangeetha S. AMMU: a survey of transformer-based biomedical pretrained language models. *J Biomed Inform* 2022;**126**:103982. https://doi.org/10.1016/j.jbi.2021.103982
39. Liu P, Yuan W, Jinlan F. *et al.* Pre-train, prompt, and predict: a systematic survey of prompting methods in natural language processing. *ACM Comput Surv* 2023;**55**:1–35.
40. Qin G, Eisner J. Learning how to ask: Querying LMs with mixtures of soft prompts. *Proc Conf N Am Chapter Assoc Comput Linguist Hum Lang Technol* 2021;5203–12.
41. Mingrui W, Cai X, Ji J. *et al.* ControlMLLM: Training-free visual prompt learning for multimodal large language models. In: Globerson A, Mackey L, Belgrave D. *et al.* (eds.), *Advances in Neural Information Processing Systems* 37, pp. 45206–34. Red Hook, NY: Curran Associates, Inc., 2024.
42. Wang Y, Jiao Q, Wang J. *et al.* Prediction of protein-ligand binding affinity with deep learning. *Comput Struct Biotechnol J* 2023;**21**:5796–806. https://doi.org/10.1016/j.csbj.2023.11.009
43. Ghandikota SK, Jegga AG. Chapter seven—Application of artificial intelligence and machine learning in drug repurposing. In: Singh V (ed.), *New Approach for Drug Repurposing Part a (Progress in Molecular Biology and Translational Science)*, Vol. **205**, pp. 171–211. Cambridge, MA: Academic Press, 2024.
44. Volkow ND, Blanco C. The changing opioid crisis: Development, challenges and opportunities. *Mol Psychiatry* 2020;**26**:218–33.
45. Zamir SW, Arora A, Khan S. Restormer: Efficient transformer for high-resolution image restoration. In: Chellappa R, Grauman K, Hua G. *et al.* (eds.), *Proceedings of the IEEE/CVF Conference on Computer Vision and Pattern Recognition (CVPR)*, pp. 5728–39. New York, NY: IEEE, 2022.
46. Zeng X, Xiang H, Linhui Y. *et al.* Accurate prediction of molecular properties and drug targets using a self-supervised image representation learning framework. *Nat Mac Intell* 2022;**4**:1004–16. https://doi.org/10.1038/s42256-022-00557-6
47. Chithrananda S, Grand G, Ramsundar B. ChemBERTa: Large-scale self-supervised pretraining for molecular property predictionarXiv preprint arXiv:2010.09885. 2020.
48. Wang Y, Wang J, Cao Z. *et al.* Molecular contrastive learning of representations via graph neural networks. *Nat Mach Intell* 2022;**4**:279–87. https://doi.org/10.1038/s42256-022-00447-x
49. Wishart DS, Feunang YD, Guo AC. *et al.* DrugBank 5.0: a major update to the DrugBank database for 2018. *Nucleic Acids Res* 2018;**46**:D1074–82. https://doi.org/10.1093/nar/gkx1037
50. Liu J, Yang Z. Test-time adaptation for real-world video adverse weather restoration with meta batch normalization. *IEEE Trans Circuits Syst Video Technol* 2025;**35**:5533–44. https://doi.org/10.1109/TCSVT.2025.3526998
51. Ma J, Sheridan RP, Liaw A. *et al.* Deep neural nets as a method for quantitative structure-activity relationships. *J Chem Inf Model* 2015;**55**:263–74. https://doi.org/10.1021/ci500747n
52. Lavecchia A. Machine-learning approaches in drug discovery: methods and applications. *Drug Discov Today* 2015;**20**:318–31. https://doi.org/10.1016/j.drudis.2014.10.012
53. Chen H, Engkvist O, Wang Y. *et al.* The rise of deep learning in drug discovery. *Drug Discov Today* 2018;**23**:1241–50. https://doi.org/10.1016/j.drudis.2018.01.039
54. Zhavoronkov A, Ivanenkov YA, Aliper A. *et al.* Deep learning enables rapid identification of potent DDR1 kinase inhibitors. *Nat Biotechnol* 2019;**37**:1038–40. https://doi.org/10.1038/s41587-019-0224-x
55. Vamathevan J, Clark D, Czodrowski P. *et al.* Applications of machine learning in drug discovery and development. *Nat Rev Drug Discov* 2019;**18**:463–77. https://doi.org/10.1038/s41573-019-0024-5
56. Askr H, Elgeldawi E, Ella HA. *et al.* Deep learning in drug discovery: an integrative review and future challenges. *Artif Intell Rev* 2023;**56**:5975–6037. https://doi.org/10.1007/s10462-022-10306-1
57. Zhenqin W, Ramsundar B, Feinberg EN. *et al.* MoleculeNet: a benchmark for molecular machine learning. *Chem Sci* 2018;**9**:513–30.
58. Jayatunga MKP, Ayers M, Bruens L. *et al.* How successful are AI-discovered drugs in clinical trials? A first analysis and emerging lessons. *Drug Discov Today* 2024;**29**:104009. https://doi.org/10.1016/j.drudis.2024.104009

59. Niazi SK, Mariam Z. Artificial intelligence in drug development: reshaping the therapeutic landscape. *Ther Adv Drug Saf* 2025;**16**:20420986251321704. https://doi.org/10.1177/20420986251321704
60. Tan J, Zhang Y. ExplainableFold: Understanding alphafold prediction with explainable AI. In: Jagadish HV, Karypis G, Leskovec J. *et al.* (eds.), *Proceedings of the 29th ACM SIGKDD Conference on Knowledge Discovery and Data Mining*, pp. 2166–76. New York, NY: Association for Computing Machinery, 2023.
61. Peeters MC, van Westen GJP, Li Q. *et al.* Importance of the extracellular loops in G protein-coupled receptors for ligand recognition and receptor activation. *Trends Pharmacol Sci* 2011; **32**:35–42. https://doi.org/10.1016/j.tips.2010.10.001
62. Abramson J, Adler J, Dunger J. *et al.* Accurate structure prediction of biomolecular interactions with Alphafold 3. *Nature* 2024;**630**: 493–500. https://doi.org/10.1038/s41586-024-07487-w
63. Pereira GP, Gouzien C, Souza PCT. *et al.* Challenges in predicting PROTAC-mediated protein–protein interfaces with alphafold reveal a general limitation on small interfaces. *Bioinf Adv* 2025;**5**:vbaf056.
64. Hoegen P, Dijkhof LR, Rönkkö TKE. *et al.* Deep learning in GPCR drug discovery: Benchmarking the path to accurate peptide binding. *Brief Bioinform* 2025;**26**:bbaf186.
65. Tanoli Z, Fernández-Torras A, Özcan UO. *et al.* Computational drug repurposing: approaches, evaluation of in silico resources and case studies. *Nat Rev Drug Discov* 2025;**24**:521–42. https://doi.org/10.1038/s41573-025-01164-x

© The Author(s) 2025. Published by Oxford University Press. This is an Open Access article distributed under the terms of the Creative Commons Attribution-NonCommercial License (https://creativecommons.org/licenses/by-nc/4.0/), which permits non-commercial re-use, distribution, and reproduction in any medium, provided the original work is properly cited. For commercial re-use, please contact reprints@oup.com for reprints and translation rights for reprints. All other permissions can be obtained through our RightsLink service via the Permissions link on the article page on our site—for further information please contact journals.permissions@oup.com.
Briefings in Bioinformatics, 2025, **26(6)**, bbaf636
https://doi.org/10.1093/bib/bbaf636
Problem Solving Protocol